ACS Photonics

Article

pubs.acs.org/journal/apchd5

Directional Emission from Leaky and Guided Modes in GaAs Nanowires Measured by Cathodoluminescence

Benjamin J. M. Brenny,[†] Diego R. Abujetas,[‡] Dick van Dam,[§] José A. Sánchez-Gil,[‡] Jaime Gómez Rivas,[§,⊥] and Albert Polman*[,†]

[†]Center for Nanophotonics, FOM Institute AMOLF, Science Park 104, 1098 XG Amsterdam, The Netherlands

[‡]Instituto de Estructura de la Materia (IEM-CSIC), Consejo Superior de Investigaciones Científicas, Serrano 121, 28006, Madrid, Spain

[§]COBRA Research Institute, Eindhoven University of Technology, P.O. Box 513, 5600 MB Eindhoven, The Netherlands

[⊥]FOM Institute DIFFER, P.O. Box 6336, 5600 HH Eindhoven, The Netherlands

Supporting Information

ABSTRACT: We measure the polarization-resolved angular emission distribution from thin and thick GaAs nanowires (diameters ∼110 and ∼180 nm) with cathodoluminescence polarimetry. The nanowires, which horizontally rest on a thin carbon film, are excited by a 5 keV electron beam and emit band gap luminescence at a central wavelength of 870 nm. The emission can couple to different waveguide modes that propagate along the wire, are dependent on the wire diameter, and determine the directionality and polarization of the emission. Although each measured nanowire can support different modes, the polarized emission is dominated by the TM01 waveguide mode in all cases, independently of wire diameter. When exciting the nanowires close to the end facets, the thin and thick wires exhibit opposite directional emission. The emission from thin nanowires is dominated by a leaky TM01 mode that leads to emission toward the opposite end facet (emission to the right when exciting the left-side edge). For the thick wires, however, the TM01 mode is guided but also lossy due to absorption in the substrate. In such a case, the wires emit toward the excited end facet (to the left when exciting the left-side edge). The emission directionality switches for nanowire diameters in the range of 145−170 nm. We show that the measurements agree well with both a simple 1D current model and numerical simulations. The high spatial resolution of angle- and polarization-resolved cathodoluminescence spectroscopy provides detailed insight into the nanoscale emission and propagation of light in semiconductor nanowires.

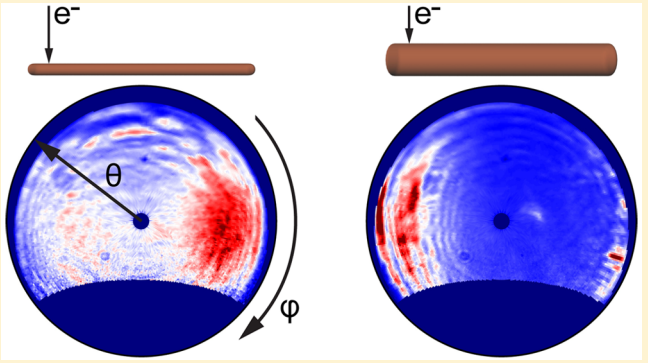

KEYWORDS: *cathodoluminescence, nanowires, GaAs, polarimetry, waveguide modes*

Semiconductor nanowires have fueled a growing field of integrated nanoscale optoelectronic devices, such as lasers,[1−3] light-emitting diodes,[4,5] photovoltaics,[6−9] single-photon detectors,[10−13] photodetectors,[14] and metamaterials.[15,16] Both the electrical and optical properties of nanowires are eminently tunable by controlling their size, geometry, or composition, among others.[17−20] The directionality and polarization of emitted radiation from nanowires have been examined in previous studies[14,21−23] and result from the coupling to leaky and guided waveguide modes,[24−29] which can also be described by Mie and Fabry-Pérot resonances.[29,30] All modes are highly dependent on nanowire diameter.

Most previous studies of semiconductor nanowire emission properties have employed optical excitation methods. While powerful, such techniques lack the nanoscale spatial resolution to uncover all the features of the radiative processes from these nanostructures. Here we use cathodoluminescence (CL) spectroscopy, in which an electron beam acts as a highly localized excitation source and the emitted light is detected.[31−33] The high spatial excitation resolution of CL is typically determined by the electron beam spot size and the evanescent field extent about the beam path (∼10−30 nm),[33] which enables the study of the nanoscale modal behavior of light.[34−37] In general, CL also allows the characterization of a wide range of material properties.[38−40] Recently, the ability to measure both the angular and polarization distribution in CL has been demonstrated.[41,42]

In this article, we use these new CL features to investigate the angle- and polarization-dependent emission from horizontal GaAs nanowires.[41] We study nanowires of different lengths and diameters that support both leaky and guided modes. Exciting the nanowires along their length, we find that the TM01 mode dominates the polarization-resolved emission for all excited

Received: January 25, 2016

DOI: 10.1021/acsphotonics.6b00065
ACS Photonics XXXX, XXX, XXX−XXX

wires, but depending on the diameter, the mode is either leaky or guided. We observe a distinct change of the directionality of the CL emission when exciting the nanowires close to their end facets, which correlates with the nanowire diameter and the nature of the mode. Thinner, leaky wires emit in the opposite direction from thicker, guided wires. The measurements exhibit good agreement with both a simple 1D current model and numerical simulations, which show that the substrate also plays a role in the emission directionality.

EXPERIMENT

GaAs nanowires were grown by self-catalyzed molecular beam epitaxy on silicon[43,44] and were subsequently mechanically broken and deposited on a holey carbon TEM grid (see Methods). Scanning electron micrographs of the two GaAs nanowires studied here are shown in Figure 1a. The thin NW1 has a length of 7.9 μm and a diameter of 100−120 nm, while the thick NW2 has a length of 12 μm and a diameter of 175−195 nm. Both wires are slightly tapered, the right-hand side being thinner, although NW2 does thicken again slightly at the very edge. The nanowires lie horizontally on the ∼20 nm thick carbon layer. In the Supporting Information we show data for an additional thin and thick wire (SEM images shown in Figure S1).

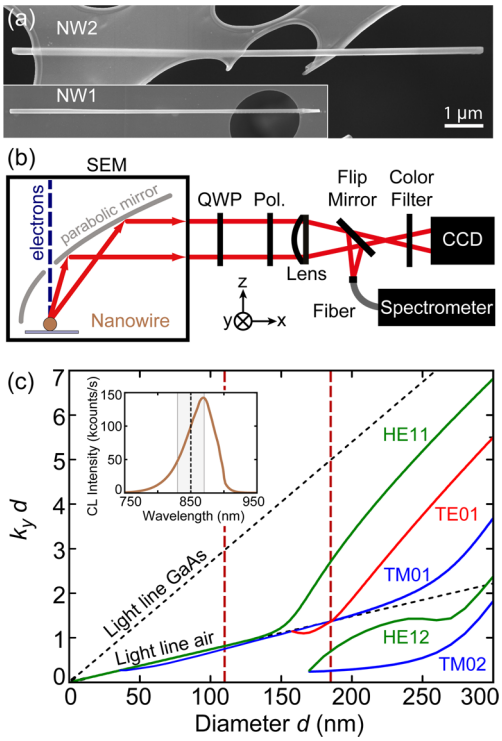

Figure 1. (a) Scanning electron micrographs of the GaAs nanowires NW1 (bottom) and NW2 (top), shown on the same scale. NW1 is 7.9 μm long and 100−120 nm thick; NW2 is 12 μm long and 175−195 nm thick. (b) Schematic overview of the cathodoluminescence polarimetry setup. The electron beam excites the nanowires, and the emitted radiation is collected by a parabolic mirror and either focused onto a fiber connected to a spectrometer or sent through a QWP, linear polarizer, and bandpass filter before being imaged onto a 2D CCD camera. (c) Dispersion relation of leaky and guided modes for infinitely long cylinders, showing the real part of the wavevector k_y multiplied by the cylinder diameter d, as a function of d, for GaAs at λ_0 = 850 nm (n = 3.6, k_0 = 7.39 μm^{-1}). The vertical red dashed lines indicate the average diameters of the two wires. The inset shows the measured CL emission spectrum from NW2. The spectrum of NW1 (not shown) does not differ noticeably except for a lower intensity. The vertical black dashed line in the inset at λ_0 = 850 nm indicates the transmittance maximum of the bandpass filter used for the angular measurements, while the gray area indicates the 40 nm bandwidth of the filter.

The cathodoluminescence spectroscopy and polarimetry setup[41,45,46] is schematically shown in Figure 1b. A parabolic mirror collects the radiation from the nanowires and directs it onto a spectrometer or images it onto a 2D camera to measure the angular intensity distribution for a given wavelength (using a bandpass filter). Polarization-resolved measurements are obtained by using a polarimeter composed of a quarter-wave plate (QWP) and a linear polarizer, which determines the Stokes parameters of the emitted radiation. The full polarization can be detected in this way, obtaining information about the degree of polarization and its orientation, ellipticity, and handedness. Essentially, this allows the retrieval of any arbitrary polarization state, including the different electric field components and the phase difference between them.[47] This is not possible using only a linear polarizer. We correct for the geometrical and polarization-dependent transformations of the parabolic mirror on the measured emission[41] (see Methods for more details about the CL measurements). For the measurements, the nanowires are aligned along the y-axis, as defined by the coordinate system shown in Figure 1b. As we expect directional emission along the nanowire axis, this is the preferred orientation for the mirror to collect the radiation symmetrically. The CL emission spectrum from NW2 is shown in the inset of Figure 1c and is dominated by band gap recombination centered around λ_0 = 870 nm. This emission can feed into waveguide modes supported by the nanowire, which depend on its diameter and which can affect the polarization and directionality of the emitted radiation.[22−24,28]

NANOWIRE WAVEGUIDE MODES

Figure 1c shows the dispersion relation of waveguide modes for infinitely long cylinders,[48] calculated for GaAs at λ_0 = 850 nm (n = 3.6, k_0 = 7.39 μm^{-1}), the wavelength at which we filter the angle-resolved measurements. We follow the formalism used in ref 27 and determine the wavevector k_y along the axis of the nanowire. We show the real part of k_y multiplied by the wire diameter d, as a function of d. The dispersion curves denote transverse electric (TE), transverse magnetic (TM), and magnetoelectric (HE) modes. These modes are characterized as "leaky" if their dispersion lies below the light line of air ($k_y < k_0$), in which case they also possess a non-negligible imaginary part of the wavevector k_y.[27] If the mode dispersion lies above the light line of air but below the light line in GaAs ($k_{GaAs} > k_y > k_0$), the waveguide mode is guided within the nanowire.

The vertical red dashed lines in Figure 1c display the average diameter of the two nanowires studied here. For the thin NW1 (and any nanowire with a diameter below 150 nm), only the TM01 and the HE11 modes are supported. Both are very close to the light line in air, but the TM01 mode is slightly below it and thus leaky for these diameters. In the case of the thicker NW2, the TE01, HE12, and TM02 also occur. The latter two are far below the light line in air and thus have a very short propagation length along the nanowire, while the HE11 mode is very clearly guided. The TE01 and TM01 modes are both very close to the light line of air in this region, representing a transition region between a leaky and guided nature for these modes. Which modes will dominate the emission depends on

DOI: 10.1021/acsphotonics.6b00065
ACS Photonics XXXX, XXX, XXX−XXX

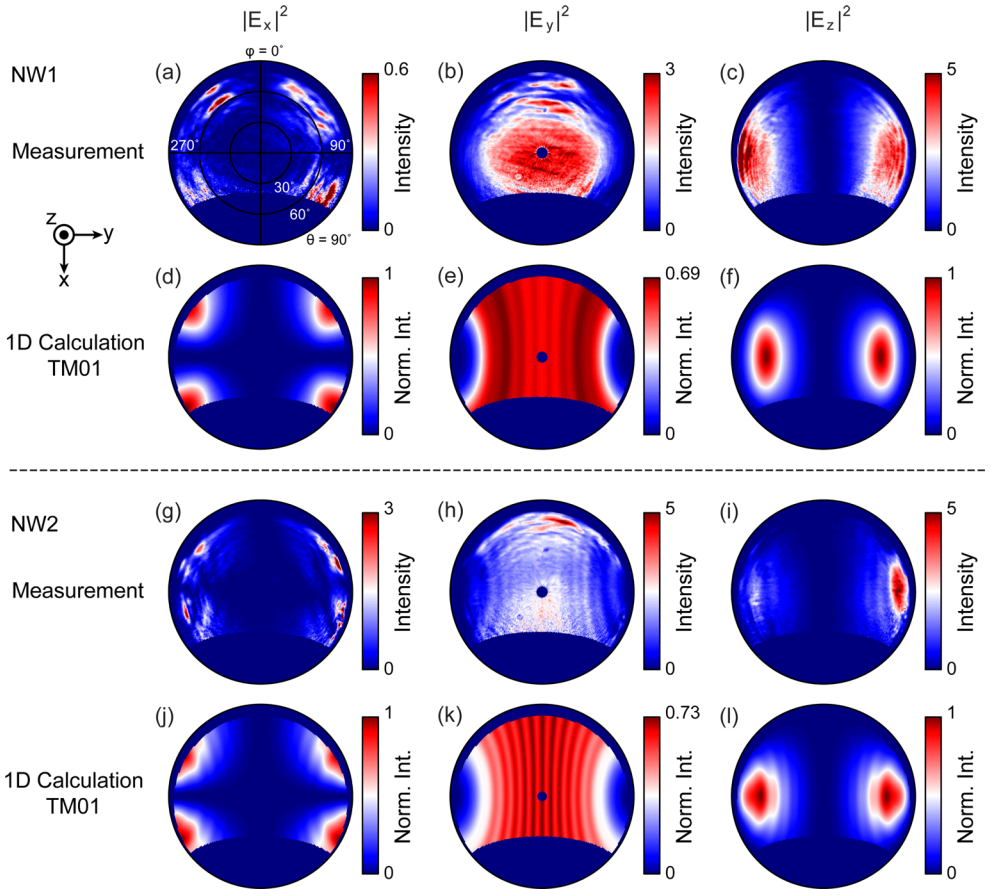

Figure 2. Measured (a–c, g–i) and calculated (d–f, j–l) angular emission distributions of the Cartesian field intensities at λ_0 = 850 nm for NW1 (a–f) and NW2 (g–l), as a function of azimuthal (φ) and zenithal (θ) angles. The patterns were measured and calculated for central excitation of the nanowires. (a, d, g, j) Intensity of the E_x field component; (b, e, h, k) intensity of E_y; and (c, f, i, l) intensity of E_z (the coordinate system is shown in the top left). The calculations for each wire determine the far-field emission profiles for the TM01 mode. We use the full range of the color scale for each panel, but the intensity scales for all three field components of each nanowire are normalized to the maximum value (E_x and E_z are equal). The measured intensities are given in 10^6 counts sr^{-1} s^{-1}.

the coupling efficiency between the excitation source and the mode.

The dispersion relation allows us to determine which modes can play a role in the emission from these nanowires and to calculate the wavevector corresponding to each mode for a given diameter. A 1D current model, developed in ref 27 and applied in ref 23, uses the wavevectors to calculate far-field emission patterns for all electromagnetic field components. The model describes the nanowire as a 1D cavity in vacuum with length L; the emission is produced by a line current excited by a dipole at a given position along the wire. This simple model allows us to retrieve the expected polarization-dependent angular emission patterns for different modes at different wire diameters, which we can compare to measurements.

CL POLARIMETRY

Measurements and calculations of the angle- and polarization-dependent emission intensity distributions at λ_0 = 850 nm for central excitation of the two nanowires clearly identify the TM01 mode as being the dominant contribution, as shown in Figure 2. For NW1 we compare the measurements (Figures 2a–c) to the 1D calculation for the TM01 mode (Figures 2d–f), displaying the Cartesian electric field intensities $|E_x|^2$, $|E_y|^2$, and $|E_z|^2$ as a function of azimuthal (φ) and zenithal (θ) angles. The field orientations are indicated by the coordinate system at the left, and the wires are oriented along the y-axis. A wavevector of k_y = 6.63 + i1.19 μm^{-1} was used for the calculation, as determined from the dispersion relation and nanowire diameter. The dark blue regions around the edges of each image correspond to the angles at which no light is collected by the mirror. The intensity scale is chosen so as to maximize the contrast in the color scale to better view the details of the features. In the case of the calculation, the intensities are normalized to the overall maximum value for each wire. We observe excellent qualitative agreement between measurement and calculation. For $|E_x|^2$ (Figure 2a,d) there are four bright features at large zenithal angles, while $|E_y|^2$ (Figure 2b,e) displays bright emission in the center of the mirror and $|E_z|^2$ (Figure 2c,f) exhibits two lobes to the left and right of the polar image, in the directions of the end facets of the nanowire.

For NW2 we also observe very similar features for both measurements (Figure 2g–i) and calculations (Figure 2j–l). A wavevector of k_y = 8.00 + i0.50 μm^{-1} was used for the calculation in this case. For $|E_x|^2$ (Figure 2g,j) we observe four features at slightly higher zenithal angles than for NW1, at the corners of the angular range. $|E_y|^2$ (Figure 2h,k) shows the brightest intensity in the center, as for NW1, but this time we can also see intensity fringes along the vertical direction, which are due to interference between the emission from the nanowire end facets. The fringes are clearly visible in the

DOI: 10.1021/acsphotonics.6b00065
ACS Photonics XXXX, XXX, XXX–XXX

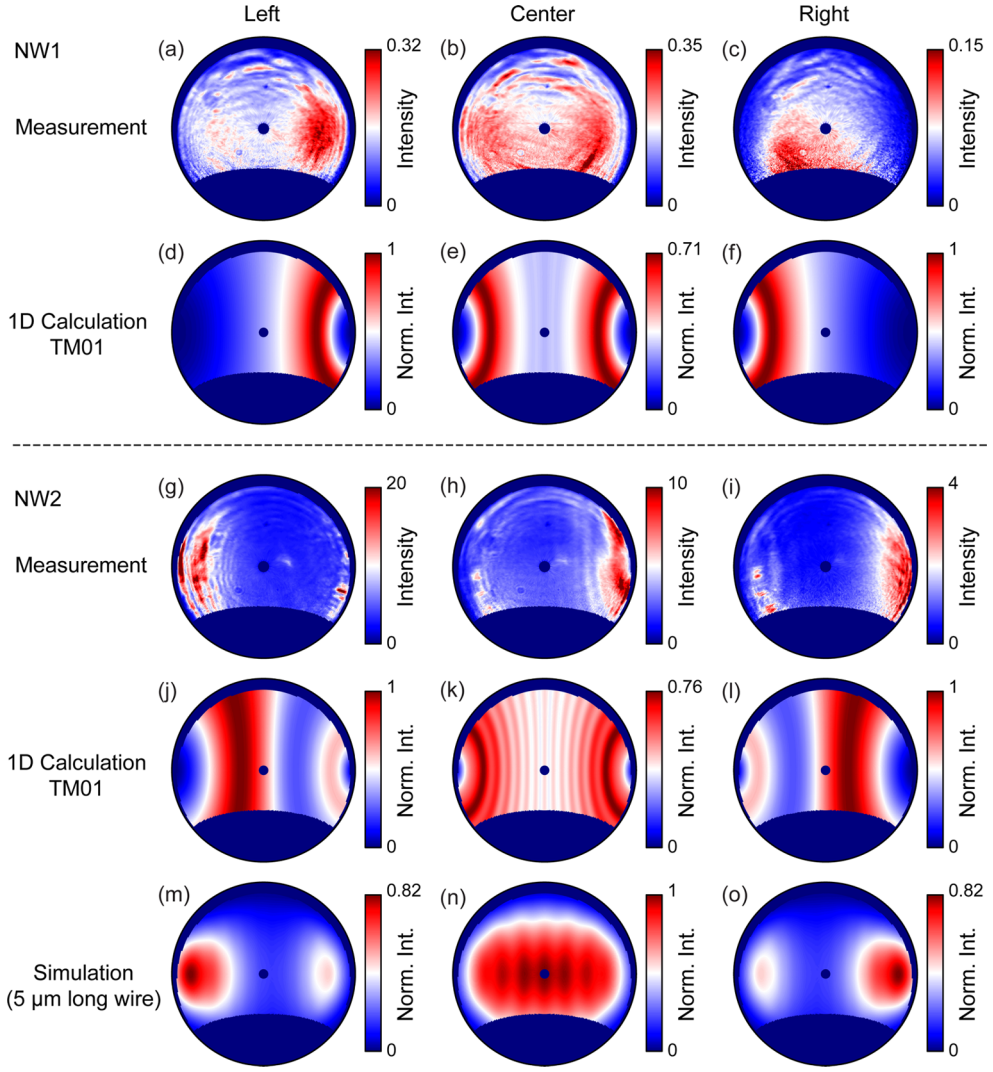

Figure 3. Measured (a–c, g–i), calculated (d–f, j–l), and simulated (m–o) angular emission distributions of the total intensity at λ_0 = 850 nm for NW1 (a–f) and NW2 (g–o). The patterns were measured and calculated for excitation at the left (a, d, g, j, m), center (b, e, h, k, n), and right (c, f, i, l, o) of the nanowires (see Figure 4 for positions). The calculations and simulations for each wire have been normalized to their maximum. The measured intensities are given in 10^6 counts sr^{-1} s^{-1}. The 1D calculation uses the same wire lengths as in the experiment (7.9 and 12 μm), but due to computational constraints the simulated NW2 is shorter (5 μm).

experiment, but with lower contrast than in the calculations, which we attribute to imperfections in the mirror and the nanowire end facets and to limitations on the angular resolution. Finally, $|E_z|^2$ (Figure 2i,l) again displays two lobes to the left and right, but at higher angles than for NW1, similarly to the behavior of $|E_x|^2$. In the experiment, the two lobes are asymmetric, which we attribute to the slight tapering of the wire. The emission is brighter in the direction of the thinner side. Comparing the relative intensities of calculations and measurements for both nanowires, we find that $|E_x|^2$ is weaker in the measurements than in the calculations. We ascribe this discrepancy to a lower collection efficiency at the edges of the mirror, where the $|E_x|^2$ component is strongest.

Even though the two nanowires have quite different diameters, in both cases we can clearly recognize very similar polarized field distributions that show excellent qualitative agreement with calculations for the TM01 mode. From this we conclude that the emission behavior of both NW1 and NW2 is dominated by the TM01 mode. The fundamental HE11 mode does not appear to play a major role in our case. This has been observed previously[22] and is ascribed to the fact that the fields are localized more outside of the wire for the HE11 mode than for the TM01 mode, which shows relatively more intensity in the center of the wire, allowing it to couple more strongly. For comparison, we include calculations of the far-field emission profiles of the HE11 mode for central excitation of the thin and thick nanowires in Figure S4 of the Supporting Information. Examining all field components, we find there is much better agreement with the TM01 mode than with the HE11 mode. This confirms that the CL emission couples most efficiently to the TM01 mode. Differences between the two wires are expected, however, because for NW1 the mode is leaky ($\mathrm{Re}(k_y)$ = 6.63 < k_0 = 7.39 μm^{-1}), while for NW2 it is guided ($\mathrm{Re}(k_y)$ = 8.00 > k_0 = 7.39 μm^{-1}). To support the data, we show polarization-resolved measurements for an additional thin and thick nanowire in Figure S2 of the Supporting Information, which exhibit the same type of features for all three field components as the results shown here.

DOI: 10.1021/acsphotonics.6b00065
ACS Photonics XXXX, XXX, XXX–XXX

DIRECTIONAL EMISSION

Next, we study the directional behavior of the nanowire emission for excitation off-center, near the end facets of the wires, observing a distinct difference in the directionality of the emission between NW1 and NW2, as shown in Figure 3. We compare the total intensity that both wires emit as a function of the azimuthal and zenithal angles in the case of measurements, calculations, and simulations, for excitation at the left edge, center, and right edge. The edge excitation is always a few hundred nanometers away from the end facet, with the exact positions shown by the dashed lines in Figure 4. We compare the total intensity measurements to calculations using the dominant TM01 mode. Polarimetry measurements for select positions near the end facets (not shown here) display the same characteristic features as in Figure 2, so we do not observe a transition to a different mode at the edges. The measured intensities differ between the wires and excitation positions, which we attribute to variations in local material quality and size of the interaction volume (due to tapering and different diameters). Here the total emission intensity is brighter when exciting the thicker ends. For the measurements on NW1, central excitation (Figure 3b) results in two symmetric lobes of higher intensity to the left and right, while excitation at the left edge (Figure 3a) leads to directional emission to the right side and excitation on the right (Figure 3c) leads to emission toward the left side. 1D calculations of the total emission intensity from the leaky TM01 mode qualitatively reproduce the emission behavior for excitation in the center and 300 nm from the end facets (Figure 3d–f). In the measurements, the electron beam excitation at the edges was ∼300–500 nm from the end facets.

We attribute the discrepancies in the shape of the emission patterns between measurements and calculations to the fact that the excitation volume can be much larger than the electron beam width (up to a few hundred nanometers). This is due to electron scattering, secondary electron generation, carrier diffusion, and photon recycling, which can play a large role in such a direct band gap material.[42,49,50] A large majority of excitations occur very close to the point of impact, but light generation will cover a larger area. The overall spatial resolution is determined by a convolution of all of these effects and will depend on the material properties. For such strongly luminescent materials as GaAs the resolution is not as good as the electron beam size but better than the full interaction volume. This is different from the calculations, which assume a point-source. The presence of the thin holey carbon substrate, which is not taken into account in the calculation, can also affect the emission, as we will now show for NW2.

The measurements on the thicker NW2 (Figure 3g–i) show the opposite directionality to that of NW1. Excitation at the left edge leads to emission toward the left, while excitation at the right edge produces emission toward the right. The excitation positions were 700 nm (left) and 400 nm (right) away from the end facets (see also the dashed lines in Figure 4b). For central excitation we observe asymmetrical emission, as was the case for Figure 2i, which we again attribute to the tapering of the wire that creates an inherent asymmetry in the wire and its emission properties. The tapering affects the leaky mode in the thin wire less since radiation is emitted continuously as the mode propagates along the wire. The thicker NW2, on the other hand, supports a guided mode, so light mostly escapes from the end facets and has a longer propagation length, traveling through the wire for multiple round trips. Since the modal properties are very sensitive to the diameter, the gradual variations along the length of the wire will affect the light more strongly.

We first compare the measurements to the 1D calculations of the (guided) TM01 mode, which do not directly take the substrate into account (Figure 3j–l). We represent absorption at the band edge and losses into the substrate by an imaginary part of k_y of 0.50 i μm^{-1}; this leads to an effective absorption length of 2 μm, much larger than the TM01 wavelength (∼220 nm), but shorter than the NW length, thus limiting mode bouncing at the NW edges. We find that for excitation near the edges (500 nm away from the end facet, similarly to the measurement) there is a maximum in emission to the same side as in the measurements, with a weaker feature in the opposite direction. We note that in the measurements of NW2 there is also a region of higher intensity to the opposite side of the dominant emission. For central excitation, we observe quite good qualitative agreement between experiment and calculation, taking into account the asymmetry we attribute to tapering of the wire. As shown in Figure 3k, interference fringes from the emission of both facets are expected for this long wire. These are also faintly visible in Figure 3h.

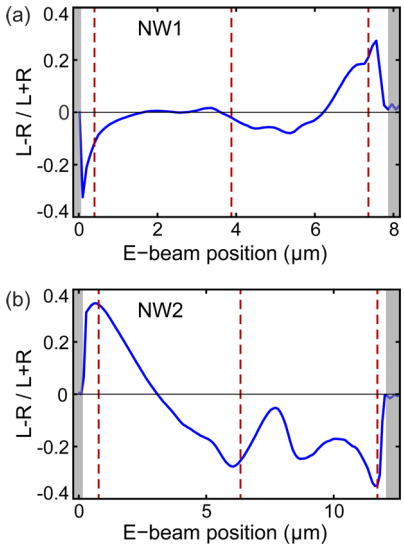

Figure 4. Ratio of the left-to-right directional emission for NW1 (a) and NW2 (b), showing the ratio (L − R)/(L + R) as a function of the electron beam position as it scans along the wire. The gray bands indicate positions that are not on the wire, while the red dashed lines indicate the positions of the left, center, and right measurements shown in Figure 3. The leftward and rightward directional intensities were determined by averaging the total intensity over all zenithal angles in 60° azimuthal wedges (ϕ = 240–300° for left and ϕ = 60–120° for right).

To get a better measure for the effect of the substrate, we perform numerical simulations using COMSOL (see Methods for more details) on a 180 nm thick and 5 μm long wire on a semi-infinite carbon substrate (Figure 3m–o). Due to computational constraints, we did not simulate a 12 μm long wire nor the extremely thin substrate. The simulations, however, do show good qualitative agreement with the experiment and provide insight into the role of the substrate on the emission behavior. Central excitation leads to a symmetric emission profile with highest intensity in the central region and interference fringes that are less distinct than for the

DOI: 10.1021/acsphotonics.6b00065
ACS Photonics XXXX, XXX, XXX–XXX

1D calculation. Excitation at the edges (500 nm from the end facets) shows emission profiles in good qualitative agreement with the measurements. There is a bright feature on the same side at high angles and a weaker spot on the opposite side. Both the 1D calculations and the simulations predict the measured directionality, which is completely opposite to the behavior of NW1. The features measured for edge excitation closely resemble the simulation, while there is better agreement with the 1D calculation for central excitation. As the substrate is very thin, we can expect it to have a smaller effect than in the simulation that was performed for a semi-infinite substrate. The importance of the substrate as an additional loss channel does not play a large role in the case of the leaky mode ($k_y < k_0$), as there is already a strong inherent leakage. For the thicker wire, simulations without substrate show an emission directionality that is more strongly dependent on excitation position and near the edges becomes opposite to that observed in the measurements (Figures S4 and S5 in the Supporting Information). We conclude that both the guided behavior of the TM01 mode and the additional loss channel due to the substrate play a role in determining the directional emission behavior of the thick nanowire.

The changing directionality observed in the measurements and calculations may be understood in an intuitive manner, when examining the differences between leaky and guided modes. For the leaky mode, leakage of the light along the nanowire dominates the emission. When exciting close to an end facet, light propagating to the edge will partially reflect back, while light going to the opposite side will propagate longer and thus leak out more, leading to a majority of the emission into the opposite direction. For the guided mode, emission from the end facets dominates, while there is loss to absorption into the substrate for light propagating along the wire, so more light will scatter out from the closest edge than from the far edge.

We can study the directional behavior of the emission as a function of the excitation position more closely, taking advantage of the high spatial resolution of CL. As discussed previously, the resolution is not limited to the electron beam size, but still remains subwavelength. Figure 4 shows the emission directionality for both wires when scanning the beam along their length. We determine a left-to-right ratio (L − R)/(L + R) by averaging the total intensity over all zenithal angles in 60° azimuthal wedges on the left and right sides, as these correspond to the regions of highest intensity features. The gray bands correspond to positions that are outside the wires, and the dashed lines indicate the positions of the measurements in Figure 3.

Comparing NW1 (Figure 4a) to NW2 (Figure 4b), we observe that there is no left/right directionality at the very edges for both wires, but that close to the edges the left-to-right ratio reaches a maximum that is reversed for the two wires, as expected from Figure 3. Figure S6 in the Supporting Information shows the left-to-right ratio for simulations of a thick wire, which also exhibit a maximum close to the end facet. Additionally, the simulations with substrate show better agreement with the measurements than the simulations without. The directionality we observe results from interference of waves propagating back and forth in the nanowire, which is dependent on the reflection at the end facets, absorption and leakage during propagation, and also the excitation position. This peak in emission close to the end facet is convoluted with the interaction volume of the electrons with the material. At the very edge we do not excite as large a region, which contributes to the decrease in intensity and directionality we observe.

The change in emission directionality observed here is consistent with the additional thin and thick nanowires examined in the Supporting Information (Figure S3). Comparing all nanowires, the thickest diameter for the leaky behavior in the thinner wires is 145 nm, while the thinnest diameter for the guided behavior in the thicker wires is 170 nm. This indicates that the transition in emission directionality should occur for nanowire diameters in the range of 145−170 nm.

CONCLUSION

In conclusion, we have demonstrated that cathodoluminescence emission from GaAs nanowires is strongly directional and depends on the nanowire diameter. The emission excited by the electron beam couples to waveguide modes that determine the polarization and angular distribution of the outcoupled radiation. These waveguide modes are very sensitive to wire diameter, especially as they change in nature from leaky to guided when crossing the light line in air. Polarization-resolved measurements show that the TM01 mode dominates the emission from both nanowires. The thin wire supports a leaky TM01 mode, which displays emission in the direction opposite to the excited edge, while the thick wire supports a guided TM01 mode that exhibits emission in the same direction. The emission directionality switches for nanowire diameters in the range of 145−170 nm. Both the leaky/guided nature of the mode and the presence of the substrate play an important role in determining the emission directionality. Cathodoluminescence polarimetry proves to be a powerful technique to study the angular- and polarization-dependent emission properties of semiconductor nanowires or other nanostructures, with a subwavelength excitation resolution.

METHODS

Sample Fabrication. The GaAs nanowires were grown on a Si(111) undoped wafer via a Ga-assisted method in a DCA P600 solid-source MBE machine.[43,44] Typical growth parameters are as follows: a Ga rate of 0.3 Å/s as flux of 2.5×10^{-6} Torr, a substrate temperature of 640 °C, rotation of the substrate at 7 rpm, and a V/III beam equivalent pressure ratio of 50. The nanowires were removed from the silicon substrate in a 2-propanol solution by ultrasonic bath for 1 min. A few drops of the 2-propanol solution containing nanowires were transferred to a holey carbon TEM grid (Plano GmbH).

CL Measurements. The measurements were performed in a FEI XL-30 SFEG (5 keV electron beam, ∼0.1 nA current) equipped with a home-built CL system.[33,45,46] The emission excited by the electron beam is collected by an aluminum paraboloid mirror and directed to an optical setup. We measure either the spectrum using a liquid-nitrogen-cooled back-illuminated silicon CCD array (Princeton Instruments Spec-10 100B) or the angular emission profile using a Peltier-cooled back-illuminated 2D silicon CCD array (Princeton Instruments PIXIS 1024B).[45,46] Using a series of six measurements of the angular CL distribution with the 2D CCD array in conjunction with a quarter-wave plate and linear polarizer (LP) determines the full emission polarization. Each measurement was taken for a different combination of QWP and LP settings (horizontal, vertical, 45°, 135°, right- and left-handed circular). We correct for the geometrical and polarization dependent response of the

DOI: 10.1021/acsphotonics.6b00065
ACS Photonics XXXX, XXX, XXX−XXX

paraboloid mirror on the CL emission that it redirects to the optical setup.[41] A 40 nm bandpass color filter was used to spectrally select the measured emission at λ_0 = 850 nm. Integration times of 0.1−1 s were used depending on sample brightness. For every setting of the QWP and LP, we collected a dark reference measurement where we blank the electron beam (using the same integration time as for the corresponding CL measurement). This reference was subtracted from the data in the postprocessing stage. Possible sources of measurement errors include drift of the electron beam, bleaching/contamination, which leads to a reduction in CL signal, and fluctuations in the current and/or the alignment of the mirror.

FEM Simulations. The finite-element-method (FEM) simulations of the far-field emission profiles of finite nanowires were performed using the commercial sofware package COMSOL Multiphysics v4.3b, using the same methods as in refs 27 and 23. For free-standing nanowires the simulation space consisted of a circular cylinder of length L and diameter d that represents the nanowire, enclosed in three concentric spheres of diameter $L + 2\lambda_0$, $L + 4\lambda_0$, and $L + 6\lambda_0$, with their centers coinciding with that of the cylinder. The innermost two spheres were set to be air (n_{air}), while the outermost layer was defined as a perfectly matched layer (PML) to absorb all outgoing radiation and prevent reflections. The material constants of GaAs for the cylinder were taken from Palik[51] (n_{GaAs} = 3.6 at λ_0 = 850 nm). A tetrahedral mesh was used, with maximum element sizes (MES) of 25 nm in the domain of the cylinder and 160 nm for the air domains. The maximum element growth rate was set to 1.35 for all of the domains.

For nanowires on top of a carbon substrate the geometry is modified as follows. The three concentric spheres of the same diameter are divided into two semispherical layered domains through a plane that contains the cylinder axis, and the cylinder is then shifted by $d/2$ from its original position in order to be placed on top of one of the new semispherical spaces, which we refer to as the substrate. The substrate was set to be amorphous carbon (n_C = 1.987 + i0.83 at λ_0 = 850 nm),[52] and the rest was set to be air, except for the GaAs cylinder. As the space was divided into two different media, the material properties of the outermost PML must be the same as the adjacent medium. The MES of the tetrahedral mesh was 25 nm for the cylinder, 160 nm for the air, and 90 nm for the substrate. The maximum element growth rate was 1.35, the same as for the free-standing nanowires.

Simulations were highly memory-demanding; in the case of the nanowires of length L = 5 μm on top of the substrate, the calculations need ∼400 GB. Postprocessing calculations were used to determine the total radiated power at the inner spherical boundary $\sum_{int}$, defined by

$$P = \int_{\sum_{int}} \langle \mathbf{S} \rangle \cdot \mathbf{n} dS \quad (1)$$

where $\mathbf{n}$ is the outward normal unit-vector to the surface.

■ ASSOCIATED CONTENT

Supporting Information

The Supporting Information is available free of charge on the ACS Publications website at DOI: 10.1021/acsphotonics.6b00065.

Data from an additional two measured nanowires, calculated emission profiles for the HE11 mode, as well as simulations that compare the emission behavior with and without the substrate (PDF)

■ AUTHOR INFORMATION

Corresponding Author

*E-mail (A. Polman): polman@amolf.nl.

Notes

The authors declare the following competing financial interest(s): A.P. is co-founder and co-owner of Delmic BV, a startup company developing a commercial product based on the cathodoluminescence system that was used in this work.

■ ACKNOWLEDGMENTS

The authors acknowledge Clara Osorio, Mark Knight, and Toon Coenen for fruitful discussions. We also thank Mohammad Ramezani, Gözde Tütüncüoglu, Federico Matteini, and Anna Fontcuberta i Morral for providing the GaAs sample. This work is part of the Stichting voor Fundamenteel Onderzoek der Materie (FOM) as well as the Dutch Technology Foundation STW, which are financially supported by the Nederlandse Organisatie voor Wetenschappelijk Onderzoek (NWO) and the Dutch Ministry of Economic Affairs. It is also part of NanoNextNL, a nanotechnology program funded by the Dutch Ministry of Economic Affairs, part of an industrial partnership program between Philips and FOM, and is supported by the European Research Council (ERC). The Spanish Ministerio de Economía y Competitividad is also acknowledged for financial support through the grants NANOPLAS+ (FIS2012-31070) and LENSBEAM (FIS2015-69295-C3-2-P).

■ REFERENCES

(1) Huang, M. H.; Mao, S.; Feick, H.; Yan, H.; Wu, Y.; Kind, H.; Weber, E.; Russo, R.; Yang, P. Room-temperature ultraviolet nanowire nanolasers. *Science* **2001**, *292*, 1897−1899.

(2) Vanmaekelbergh, D.; van Vugt, L. K. ZnO nanowire lasers. *Nanoscale* **2011**, *3*, 2783−2800.

(3) Röder, R.; Ploss, D.; Kriesch, A.; Buschlinger, R.; Geburt, S.; Peschel, U.; Ronning, C. Polarization features of optically pumped CdS nanowire lasers. *J. Phys. D: Appl. Phys.* **2014**, *47*, 394012.

(4) Haraguchi, K.; Katsuyama, T.; Hiruma, K. Polarization dependence of light emitted from GaAs p−n junctions in quantum wire crystals. *J. Appl. Phys.* **1994**, *75*, 4220−4225.

(5) Svensson, C. P. T.; Mårtensson, T.; Trägårdh, J.; Larsson, C.; Rask, M.; Hessman, D.; Samuelson, L.; Ohlsson, J. Monolithic GaAs/InGaP nanowire light emitting diodes on silicon. *Nanotechnology* **2008**, *19*, 305201.

(6) Wallentin, J.; Anttu, N.; Asoli, D.; Åberg, I.; Magnusson, M. H.; Siefer, G.; Fuss-Kailuweit, P.; Dimroth, F.; Witzigmann, B.; Xu, H. Q.; Samuelson, L.; Deppert, K.; Borgström, M. T. InP Nanowire Array Solar Cell Achieving 13.8% Efficiency by Exceeding the Ray Optics Limit. *Science* **2013**, *339*, 1057−1060.

(7) Cui, Y.; Wang, J.; Plissard, S. R.; Cavalli, A.; Vu, T. T. T.; van Veldhoven, R. P. J.; Gao, L.; Trainor, M.; Verheijen, M. A.; Haverkort, J. E. M.; Bakkers, E. P. A. M. Efficiency enhancement of InP nanowire solar cells by surface cleaning. *Nano Lett.* **2013**, *13*, 4113−7.

(8) Krogstrup, P.; Jørgensen, H. I.; Heiss, M.; Demichel, O.; Holm, J. V.; Aagesen, M.; Nygard, J.; Fontcuberta i Morral, A. Single-nanowire solar cells beyond the Shockley-Queisser limit. *Nat. Photonics* **2013**, *7*, 306−310.

(9) Muskens, O. L.; Gómez Rivas, J.; Algra, R. E.; Bakkers, E. P. A. M.; Lagendijk, A. Design of light scattering in nanowire materials for photovoltaic applications. *Nano Lett.* **2008**, *8*, 2638−2642.

(10) Claudon, J.; Bleuse, J.; Malik, N. S.; Bazin, M.; Jaffrennou, P.; Gregersen, N.; Sauvan, C.; Lalanne, P.; Gérard, J.-M. A highly efficient

DOI: 10.1021/acsphotonics.6b00065
ACS Photonics XXXX, XXX, XXX−XXX

single-photon source based on a quantum dot in a photonic nanowire. *Nat. Photonics* **2010**, *4*, 174−177.
(11) Heiss, M.; et al. Self-assembled quantum dots in a nanowire system for quantum photonics. *Nat. Mater.* **2013**, *12*, 439−444.
(12) Bulgarini, G.; Reimer, M. E.; Bouwes Bavinck, M.; Jöns, K. D.; Dalacu, D.; Poole, P. J.; Bakkers, E. P. A. M.; Zwiller, V. Nanowire waveguides launching single photons in a gaussian mode for ideal fiber coupling. *Nano Lett.* **2014**, *14*, 4102.
(13) Reimer, M. E.; Bulgarini, G.; Akopian, N.; Hocevar, M.; Bouwes Bavinck, M.; Verheijen, M. A.; Bakkers, E. P. A. M.; Kouwenhoven, L. P.; Zwiller, V. Bright single-photon sources in bottom-up tailored nanowires. *Nat. Commun.* **2012**, *3*, 737.
(14) Wang, J.; Gudiksen, M. S.; Duan, X.; Cui, Y.; Lieber, C. M. Highly polarized photoluminescence and photodetection from single indium phosphide nanowires. *Science* **2001**, *293*, 1455.
(15) Paniagua-Domínguez, R.; Abujetas, D. R.; Sánchez-Gil, J. A. Ultra low-loss, isotropic optical negative-index metamaterial based on hybrid metal-semiconductor nanowires. *Sci. Rep.* **2013**, *3*, 1507.
(16) Ramezani, M.; Casadei, A.; Grzela, G.; Matteini, F.; Tütüncüoglu, G.; Rüffer, D.; Fontcuberta i Morral, A.; Gómez-Rivas, J. Hybrid semiconductor nanowire-metallic Yagi-Uda antennas. *Nano Lett.* **2015**, *15*, 4889−4895.
(17) Yan, R.; Gargas, D.; Yang, P. Nanowire photonics. *Nat. Photonics* **2009**, *3*, 569−576.
(18) Duan, X.; Huang, Y.; Cui, Y.; Wang, J.; Lieber, C. M. Indium phosphide nanowires as building blocks for nanoscale electronic and optoelectronic devices. *Nature* **2001**, *409*, 66−69.
(19) Gudiksen, M. S.; Lauhon, L. J.; Wang, J.; Smith, D. C.; Lieber, C. M. Growth of nanowire superlattice structures for nanoscale photonics and electronics. *Nature* **2002**, *415*, 617−620.
(20) Thelander, C.; Agarwal, P.; Brongersma, S.; Eymery, J.; Feiner, L.; Forchel, A.; Scheffler, M.; Riess, W.; Ohlsson, B.; Gösele, U.; Samuelson, L. Nanowire-based one-dimensional electronics. *Mater. Today* **2006**, *9*, 28−35.
(21) Motohisa, J.; Kohashi, Y.; Maeda, S. Far-field emission patterns of nanowire light-emitting diodes. *Nano Lett.* **2014**, *14*, 3653−60.
(22) Grzela, G.; Paniagua-Domínguez, R.; Barten, T.; Fontana, Y.; Sánchez-Gil, J. A.; Gómez Rivas, J. Nanowire antenna emission. *Nano Lett.* **2012**, *12*, 5481−5486.
(23) van Dam, D.; Abujetas, D. R.; Paniagua-Domínguez, R.; Sánchez-Gil, J. A.; Bakkers, E. P. A. M.; Haverkort, J. E. M.; Gómez Rivas, J. Directional and polarized emission from nanowire arrays. *Nano Lett.* **2015**, *15*, 4557−4563.
(24) Maslov, A. V.; Ning, C. Z. Far-field emission of a semiconductor nanowire laser. *Opt. Lett.* **2004**, *29*, 572−574.
(25) Maslov, A. V.; Bakunov, M. I.; Ning, C. Z. Distribution of optical emission between guided modes and free space in a semiconductor nanowire. *J. Appl. Phys.* **2006**, *99*, 024314.
(26) Cao, L.; White, J. S.; Park, J.; Schuller, J. A.; Clemens, B. M.; Brongersma, M. L. Engineering light absorption in semiconductor nanowire devices. *Nat. Mater.* **2009**, *8*, 643−647.
(27) Paniagua-Domínguez, R.; Grzela, G.; Gómez Rivas, J.; Sánchez-Gil, J. Enhanced and directional emission of semiconductor nanowires tailored through leaky/guided modes. *Nanoscale* **2013**, *5*, 10582−10590.
(28) Claudon, J.; Gregersen, N.; Lalanne, P.; Gérard, J.-M. Harnessing light with photonic nanowires: fundamentals and applications to quantum optics. *ChemPhysChem* **2013**, *14*, 2393−2402.
(29) Abujetas, D. R.; Paniagua-Domínguez, R.; Sánchez-Gil, J. A. Unraveling the janus role of Mie resonances and leaky/guided modes in semiconductor nanowire absorption for enhanced light harvesting. *ACS Photonics* **2015**, *2*, 921−929.
(30) Traviss, D. J.; Schmidt, M. K.; Aizpurua, J.; Muskens, O. L. Antenna resonances in low aspect ratio semiconductor nanowires. *Opt. Express* **2015**, *23*, 22771−22787.
(31) García de Abajo, F. J. Optical excitations in electron microscopy. *Rev. Mod. Phys.* **2010**, *82*, 209−275.
(32) Adamo, G.; Ou, J. Y.; So, J. S.; Jenkins, S. D.; De Angelis, F.; MacDonald, K. F.; Di Fabrizio, E.; Ruostekoski, J.; Zheludev, N. I. Electron-beam-driven collective-mode metamaterial light source. *Phys. Rev. Lett.* **2012**, *109*, 217401.
(33) Sapienza, R.; Coenen, T.; Renger, J.; Kuttge, M.; van Hulst, N. F.; Polman, A. Deep-subwavelength imaging of the modal dispersion of light. *Nat. Mater.* **2012**, *11*, 781−787.
(34) Bashevoy, M. V.; Jonsson, F.; MacDonald, K. F.; Chen, Y.; Zheludev, N. I. Hyperspectral imaging of plasmonic nanostructures with nanoscale resolution. *Opt. Express* **2007**, *15*, 11313−11320.
(35) Zhu, X. L.; Ma, J. S.; Zhang, Y.; Xu, X. F.; Wu, J.; Zhang, Y.; Han, X. B.; Fu, Q.; Liao, Z. M.; Chen, L.; Yu, D. P. Confined three-dimensional plasmon modes inside a ring-shaped nanocavity on a silver film imaged by cathodoluminescence microscopy. *Phys. Rev. Lett.* **2010**, *105*, 127402.
(36) Takeuchi, K.; Yamamoto, N. Visualization of surface plasmon polariton waves in two-dimensional plasmonic crystal by cathodoluminescence. *Opt. Express* **2011**, *19*, 12365−12374.
(37) Coenen, T.; van de Groep, J.; Polman, A. Resonant Modes of Single Silicon Nanocavities Excited by Electron Irradiation. *ACS Nano* **2013**, *7*, 1689−1698.
(38) Yacobi, B. G.; Holt, D. B. *Cathodoluminescence Microscopy of Inorganic Solids*; Springer Science & Business Media, 1990.
(39) Edwards, P. R.; Martin, R. W. Cathodoluminescence nano-characterization of semiconductors. *Semicond. Sci. Technol.* **2011**, *26*, 064005.
(40) Thonke, K.; Tischer, I.; Hocker, M.; Schirra, M.; Fujan, K.; Wiedenmann, M.; Schneider, R.; Frey, M.; Feneberg, M. Nanoscale characterisation of semiconductors by cathodoluminescence. *IOP Conf. Ser.: Mater. Sci. Eng.* **2014**, *55*, 012018.
(41) Osorio, C. I.; Coenen, T.; Brenny, B. J. M.; Polman, A.; Koenderink, A. F. Angle-resolved cathodoluminescence imaging polarimetry. *ACS Photonics* **2016**, *3*, 147−154.
(42) Brenny, B. J. M.; van Dam, D.; Osorio, C. I.; Gómez Rivas, J.; Polman, A. Azimuthally polarized cathodoluminescence from InP nanowires. *Appl. Phys. Lett.* **2015**, *107*, 201110.
(43) Russo-Averchi, E.; Heiss, M.; Michelet, L.; Krogstrup, P.; Nygard, J.; Magen, C.; Morante, J. R.; Uccelli, E.; Arbiol, J.; Fontcuberta i Morral, A. Suppression of three dimensional twinning for a 100% yield of vertical GaAs nanowires on silicon. *Nanoscale* **2012**, *4*, 1486−1490.
(44) Matteini, F.; Tütüncüoglu, G.; Potts, H.; Jabeen, F.; Fontcuberta i Morral, A. Wetting of Ga on SiOx and its impact on GaAs nanowire growth on silicon. *Cryst. Growth Des.* **2015**, *15*, 3105−3109.
(45) Coenen, T.; Vesseur, E. J. R.; Polman, A.; Koenderink, A. F. Directional emission from plasmonic Yagi Uda antennas probed by angle-resolved cathodoluminescence spectroscopy. *Nano Lett.* **2011**, *11*, 3779−3784.
(46) Coenen, T.; Vesseur, E. J. R.; Polman, A. Angle-resolved cathodoluminescence spectroscopy. *Appl. Phys. Lett.* **2011**, *99*, 143103.
(47) Born, M.; Wolf, E. *Principles of Optics: Electromagnetic Theory of Propagation, Interference and Diffraction of Light*, 7th ed.; Cambridge University Press, 1997.
(48) Stratton, J. A. *Electromagnetic Theory*; Read Books, 1941.
(49) Haegel, N. M.; Mills, T. J.; Talmadge, M.; Scandrett, C.; Frenzen, C. L.; Yoon, H.; Fetzer, C. M.; King, R. R. Direct imaging of anisotropic minority-carrier diffusion in ordered GaInP. *J. Appl. Phys.* **2009**, *105*, 023711.
(50) Demers, H.; Poirier-Demers, N.; Couture, A. R.; Joly, D.; Guilmain, M.; de Jonge, N.; Drouin, D. Three-dimensional electron microscopy simulation with the CASINO Monte Carlo software. *Scanning* **2011**, *33*, 135−146.
(51) Palik, E. D. *Handbook of Optical Constants of Solids*; Academic Press, 1998; Vol. 3.
(52) Hagemann, H.-J.; Gudat, W.; Kunz, C. Optical constants from the far infrared to the x-ray region: Mg, Al, Cu, Ag, Au, Bi, C, and Al_2O_3. *J. Opt. Soc. Am.* **1975**, *65*, 742−744.

DOI: 10.1021/acsphotonics.6b00065
ACS Photonics XXXX, XXX, XXX−XXX